SURFACE CURRENT MEASUREMENTS IN JUAN DE FUCA STRAIT USING THE SEASONDE HF RADAR

By

D.O. Hodgins[1], R.H. Goodman[2], M.F. Fingas[3], and R. Overstreet[4]

[1]Seaconsult Marine Research Ltd.
8805 Osler Street
Vancouver, B.C.

[2]Imperial Oil Resources Limited
3535 Research Way
Calgary, Alberta

[3]Environment Canada
Emergency Sciences Division
3439 River Road
Ottawa, Ontario

[4]National Oceanic and Atmospheric Administration
7600 Sand Point Way NE
Seattle, Washington 98115
U.S.A.

ABSTRACT In coastal waterways such as the Straits of Georgia and Juan de Fuca, the surface circulation is highly variable, responding to tides, winds, and density variations. Much of this variability is not predictable in the slowly-varying part of the current field, and must be accounted for statistically in parameterizing the turbulence in both hydrodynamic models and oil spill models. A good understanding of mean flow and turbulent features requires a spatial current mapping technique. In July 1992, the SeaSonde, a new 12-MHz HF radar for mapping surface currents, was deployed at two stations in Juan de Fuca Strait. Twenty-one days of surface currents in the upper 1-2 m of the water column were measured off Victoria. The features and performance of the radar are discussed, and characteristic eddy, meander and frontal features of the surface flows are illustrated. Analysis of the data for this region shows that although tide forces account for much of the observed variance, considerable kinetic energy remains in the turbulent field.

1 INTRODUCTION

SeaSonde is an integrated data acquisition and processing system for remotely mapping ocean surface currents based on CODAR (Coastal Ocean Dynamics Applications Radar) principles. The system is comprised of two or more high-frequency (HF) radar units mounted on the shoreline separated by distances of 30 to 40 km. Each radar measures the radial component of surface current field, and the radial speeds from each site are combined to produce a map of the total surface current. The surface currents are suitable for input to oil spill trajectory models (Hodgins et al., 1992).

HF radar principles for measuring surface currents are summarized in Hodgins (1991), Hardy et al. (1989), Leise (1984), and are described in detail for SeaSonde in Lipa and Barrick (1983). In the new instruments an FMCW (frequency-modulated continuous wave) signal format is used, centered at a frequency of 12.5 MHz. The radar design provides a theoretical range of just over 79 km resolved in 31 range cells. The sea echo spectra are averaged over one hour to provide stable estimates, and as a result the radars give a 1-h time average of the actual flow field, integrated over a depth of about 1.5 m. These parameters are fixed by the radar design and cannot be changed in the field.

Proc. 16th Arctic and Marine Oil Spill Program (AMOP) Technical Seminar, June 7-9, 1993, Calgary, Alberta.

The new SeaSonde HF radar system was first deployed in August of 1991 at the southern end of the Queen Charlotte Islands. Twenty-one days of hourly surface current maps were obtained over the open ocean. Although the radar was still under development at that time, the experiment was successful, and the remotely sensed currents were validated with both drifter and current meter data (Hodgins and Hardy, 1992a; Hodgins, 1992). During that experiment all raw sea echo cross-spectra were logged for post-processing, and on-site data processing was confined to checking for correct radar operation.

By the spring of 1992, development work on the prototype SeaSonde was completed and the present demonstration project was launched in late June to collect surface current information in the more sheltered, but tidally-active waters of the Straits of Juan de Fuca and Georgia. The purpose of this project was to examine the performance of the radar in a regime of low wave heights, compared with the open ocean, and highly sheared currents that vary strongly with a diurnal tidal signal. In addition, Juan de Fuca Strait is a major ship traffic route, and this location was selected to test the radar's ship spike removal algorithm. The project was jointly sponsored by Imperial Oil Resources Limited, Environment Canada, Canadian Coast Guard, the U.S. National Oceanic and Atmospheric Administration, and Seaconsult Marine Research Ltd.

2 RADAR SITING AND DATA RECOVERY

Radar Siting. One remote site radar was deployed at the Race Rocks lightstation with a second radar unit situated on Ediz Spit, at the U.S. Coast Guard airbase in Port Angeles, giving the combined coverage area illustrated in Fig. 1. Bathymetry contours are also plotted to show the bottom relief in this area. The dominant features in the coverage area are the ridge extending from Victoria, across the main axis of Juan de Fuca Strait to a point mid-way between Ediz Hook and Dungeness Spit, the constriction in channel width at Race Rocks, essentially along the radar baseline, and the extremely variable bottom relief, particularly at the eastern edge of the coverage area.

The radar at Race Rocks was powered from the 110 V diesel generator that services the light and keeper's quarters. Between June 29th and July 8th data recovery at Race Rocks was intermittent, characterized by crashes of the data acquisition program which terminated all functions. These problems were linked to the UPS, which was too sensitive to voltage fluctuations in the 110 V supply. After July 8th, the UPS was removed and most problems disappeared.

The availability of 110 V line supply at Port Angeles avoided all power problems, and the system operated without interruption except for a few instances when the mass storage devices were filled up and the system shut down awaiting re-initialization. The transmit and receive antennas were repositioned during the first few days of deployment to optimize data recovery (isolating the receive antenna as far as possible from any pattern distortion caused by some large electrical wire reels stored near the site), and after July 9th data recovery on both sides of the baseline was achieved. Key radar characteristics are summarized in Table 2.1.

Data Recovery. As noted previously, data recovery was intermittent during early July as various operational problems were solved and some communications tests were carried out. On July 9th, the antennas at Port Angeles were re-positioned to

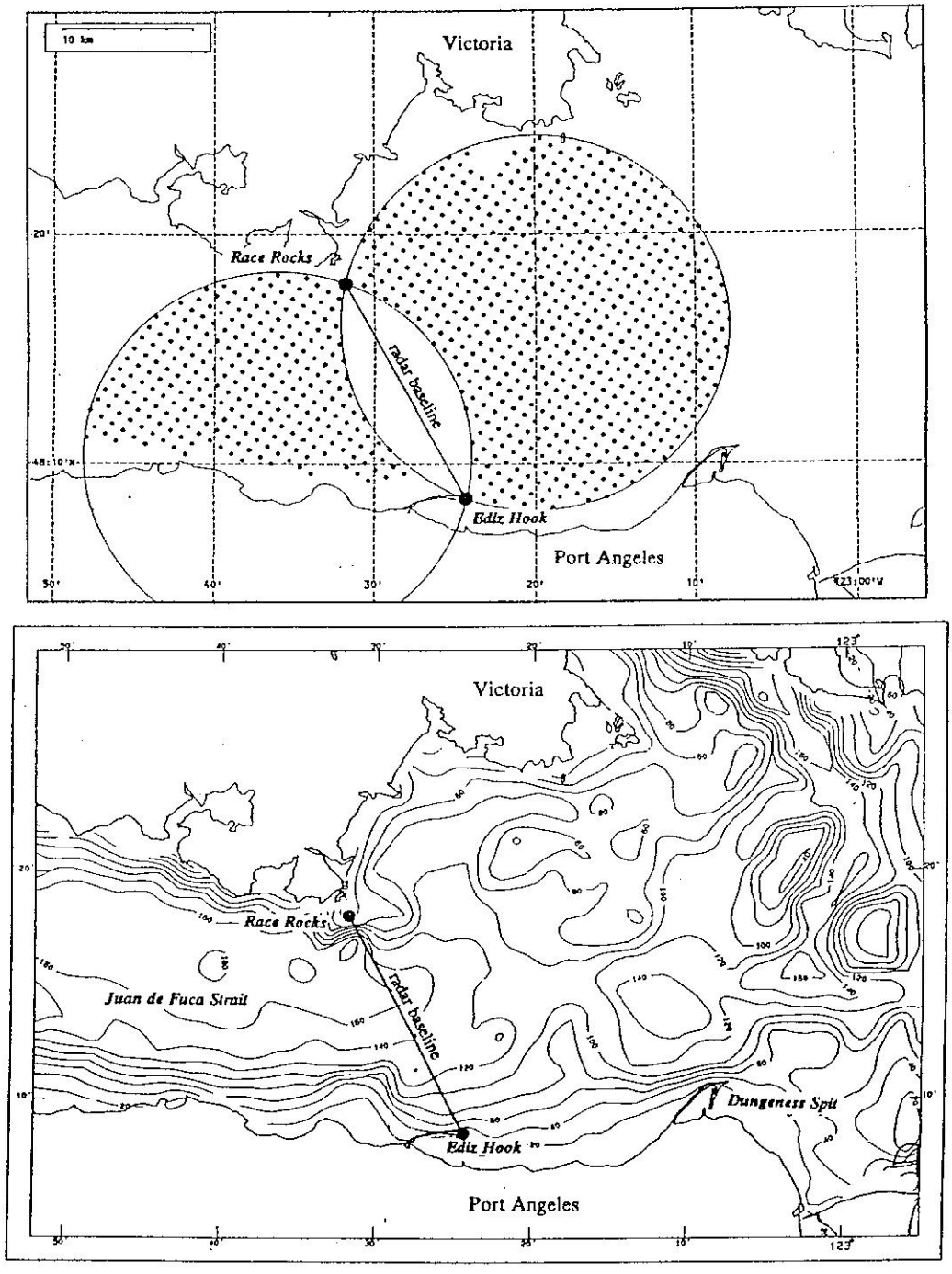

Figure 1 Site map of Juan de Fuca Strait showing the radar locations (•) and coverage area (upper panel). Bathymetry contour values in metres (lower panel).

Table 2.1: Characteristics of the SeaSonde Radars Deployed in Juan de Fuca Strait

	Race Rocks	Port Angeles
Latitude	48° 17.89' N	48° 08.50' N
Longitude	123° 31.77' W	123° 24.28' W
Sampling interval	1 h	1 h
Transmit frequency	12.421875 MHz	12.656250 MHz
Transmit power	< 100 W	< 100 W
Theoretical range	79.24 km	79.24 km
Range resolution	2.556 km	2.556 km
Radial velocity azimuth resolution	5°	5°

the end of the breakwater, improving reception and data quality, and the unit at Race Rocks began to operate reliably. The period July 9-31 provided good two-site data.

A gross measure of data recovery is given by the number of radial currents measured with each radar. In principle, given equally good siting and total aperture, both radar units should measure about equivalently in terms of range and density of derived radial current information. In this deployment the total view width at Race Rocks (approximately 270°) was wider than at Port Angeles (180°); however, antenna sheltering by the lighthouse and other structures reduced the effective width at Race Rocks to an average value closer to that at Port Angeles. As a result, the total radial current return at Race Rocks was only slightly greater than at Port Angeles.

This measure of data return is summarized in Fig. 2, where radial count at each site is plotted versus wind speed at Race Rocks. This figure shows that the return was variable but similar at both sites, indicating that factors external to the radars account for the variations rather than a characteristic of one radar site. The count data are correlated with the wind speed, which is logical, and reflects increased sea echo strength as resonant wind waves build with stronger winds. The variability shown here for Juan de Fuca Strait is slightly larger than has been experienced over the open ocean with other HF radars. This observation may be explained by the lower prevalence of resonant 12 m long waves in the strait compared with the open ocean. A higher operating frequency may decrease the variability noted here in radial returns by providing more constant range under all wind conditions.

No apparent correlation of the radial returns with tidal phase was found, although tidal currents are strong and highly modulated in this region. This outcome is also logical unless the tidal currents were modifying the wave field and thereby affecting the sea echo return. Such a modification is not expected; rather, the wave field will result from the local wind and will be closely coupled with the wind speed variations.

These results show that the 12.5 MHz radar is effective with moderate winds of 5 to 10 knots and stronger, but will suffer some loss in performance as winds abate completely and the sea becomes flat calm. Under calm conditions the radars continued to function although range is decreased, as is the dual-radar coverage area over which total currents can be derived.

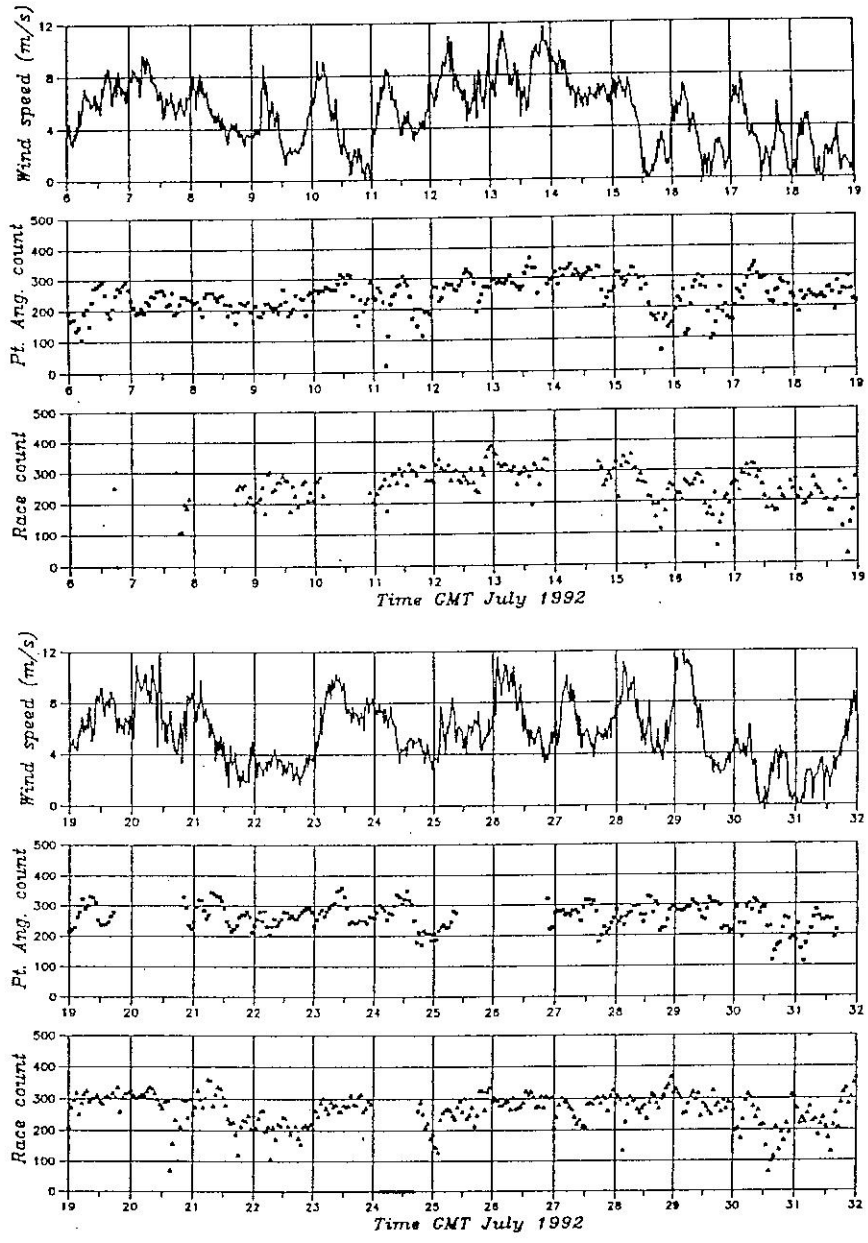

Fig. 2 Time-series of wind speed measured at Race Rocks versus radial current count from each radar site.

3 SURFACE CURRENT EXTRACTION

Radial Velocity. Radial velocities were extracted from the sea echo spectra using the least-squares method described by Lipa and Barrick (1983). This procedure statistically tested the single and dual-angle models for radial currents and selected the one having the best fit to the data. The resulting hourly radial velocity fields consisted of a variable number of range cells, each separated by 2.557 km. Within each range cell, the data records were comprised of the speed, v, and corresponding direction indicated by the sign of the speed, a parameter, δv, expressing the uncertainty associated with the speed (see Lipa and Barrick, 1983), and an angular position, given at 5° intervals.

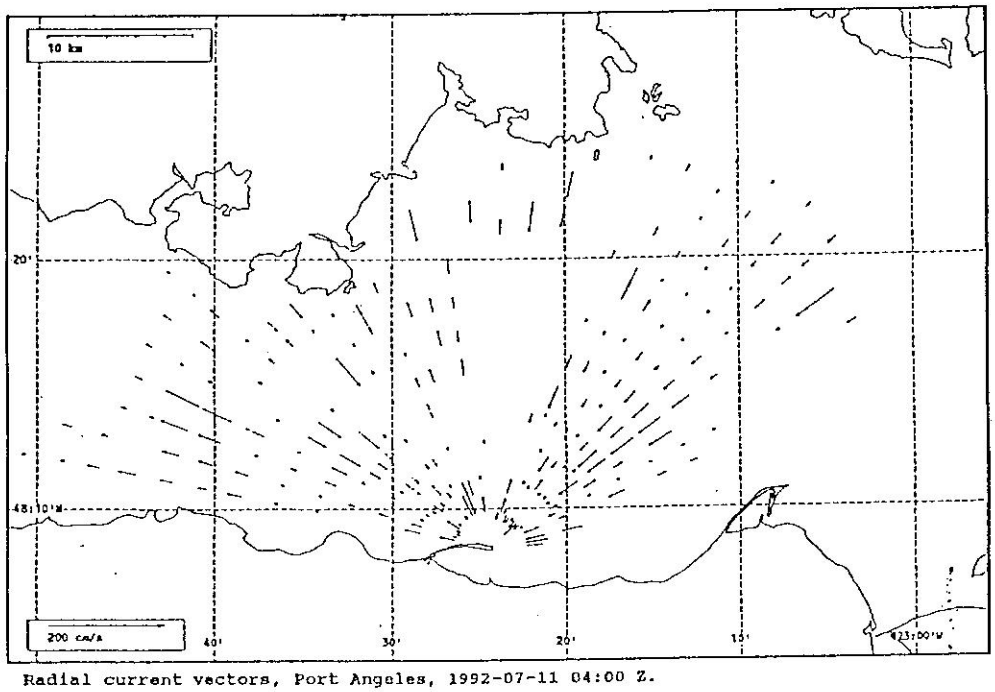

Radial current vectors, Port Angeles, 1992-07-11 04:00 Z.

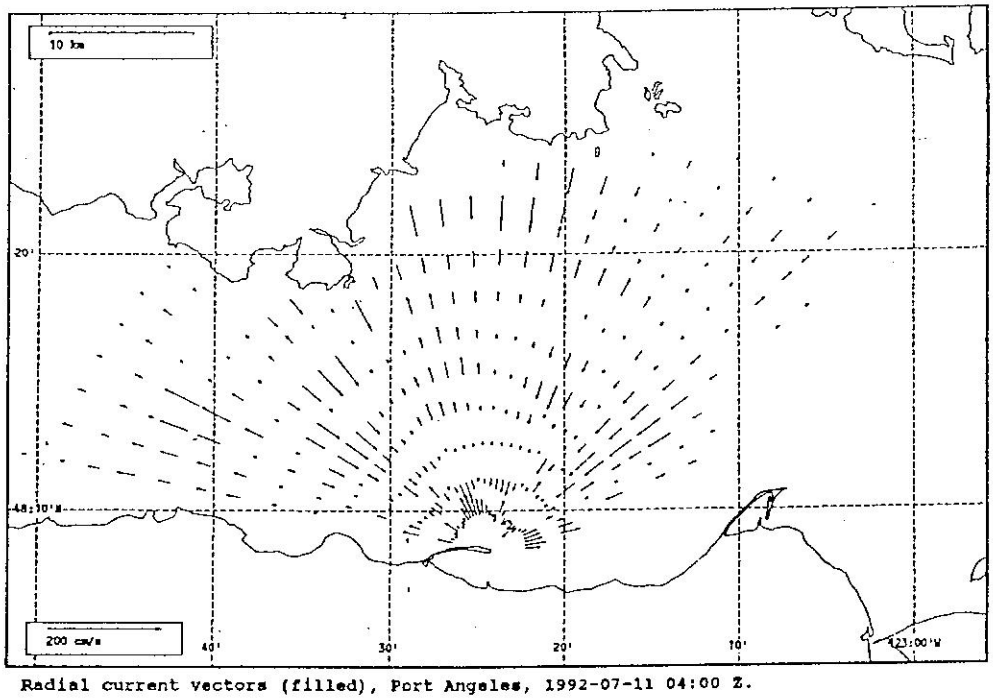

Radial current vectors (filled), Port Angeles, 1992-07-11 04:00 Z.

Figure 3 Example of radial current fields at Port Angeles before (upper panel) and after (lower panel) gap filling.

In principle, all over-water 5°-positions in the range cell should be filled if the radial speed is non-zero, but in practice there are always some gaps. In order to give optimum data recovery, the antenna phase information, used in calculation of radial currents, was estimated from the sea echo data (Lipa and Barrick, 1983) for each range ring--this is part of the standard processing algorithm. Stable phase angles for both sites were found and used to calculate the final radial current datasets.

Two thresholds were then applied to the radials to remove questionable and bad data points: (1) $\delta v > 80$ cm/s was used as the primary threshold to reject spurious radial estimates (representing less than 4% of the radial dataset), and (2) $v \geq 250$ cm/s, which exceeds the 1-hour averaged maximum current velocity that was expected anywhere within the coverage area of each radar (representing only 0.12% of all data from both sites). Finally, gaps in the radial fields were filled by interpolation, using a one-dimensional spline under tension, fitted to data within each view sector of the range ring. A view sector is an unbroken stretch of water within a single range cell, separated by land from other view sectors in the same range cell. The limiting gap width for interpolation was 10 km. No extrapolation beyond the range of data points was attempted. The interpolated radial velocities were assigned an uncertainty equal to the average δv for the data used to calculate the interpolating spline function.

There is a trade-off in processing radial data to give combined total currents between interpolation at the level of radial currents versus averaging during the combining process. Inspection of both radial and total current fields in Juan de Fuca Strait showed high spatial variability, consistent with strongly sheared flows over irregular bathymetry and around shoreline features. In consequence, gross averaging of radials together, such as has been used in previous HF radar studies (Hodgins and Hardy, 1992b; Leise, 1984) becomes increasingly inaccurate as the size of the averaging circle is increased. Given the scales of motion in Juan de Fuca Strait, more weight was given here to interpolating the radial currents to fill gaps than to averaging during the combining process.

An example of a fairly gappy radial field before and after thresholding and gap filling--illustrating the strong speed variations that were found close to the radar units--is shown in Fig. 3.

Total Current Vectors. Synchronous radial data files were combined to yield total surface current on a Cartesian grid with a resolution of 1 km applied to the study area. The two-site coverage area was constrained by placing an upper bound on the triangulation angle between vectors from the two radar sites. This bound was defined by an error factor of $\epsilon=2$ (Leise, 1984) and corresponds to angles less than 138.6° between radials or greater than 41.4° between radials.

The radial information from each radar map required to form the total current at each grid point was found by linear interpolation using the four nearest neighbours. This procedure gives better accuracy for the total current near the radar units, and becomes nearly equivalent to the blending radius method (Hodgins and Hardy, 1992) when the Cartesian grid points are further away from both radar sites. The uncertainty of the final current vector was calculated by propagation of error from the speed and δv values of the radial data that enter the interpolation procedure.

The current map in Fig. 4 is typical of many in the dataset and illustrates several oceanographically significant features; at this time, the tide is late on the rising flood limb, two hours before high water. The surface flow is characterized by spatially coherent closed eddies: one just east of Race Rocks with a diameter of about 5 km, and one southwest of Race Rocks, in mid-channel, with a diameter of approximately 7 to 8 km. Between these two eddies, flows converge around Race Rocks to form a pronounced cross-channel front. To the east of the baseline, flows exhibit a NS meandering pattern with a wavelength of about 18 to 20 km, terminating on the south in a convergent front just northeast of Port Angeles.

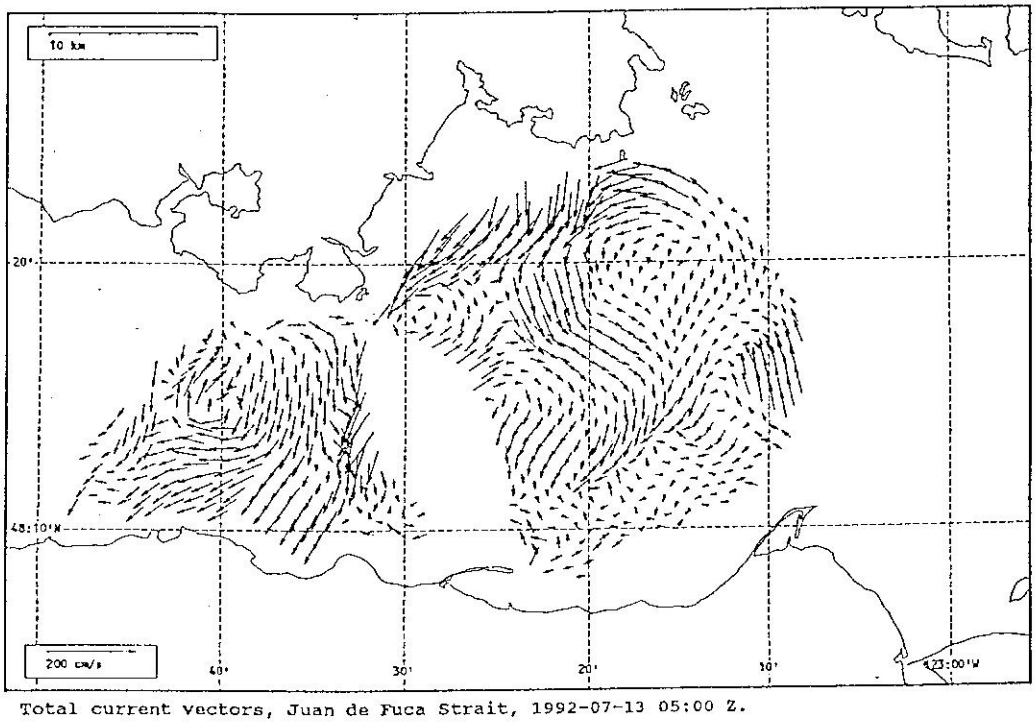

Fig. 4 Surface current map two hours before high water.

Three maps for flood tide are shown in Fig. 5a to 5c, each map at approximately the same tidal phase. It can be seen that all three maps share an overall pattern similarity, providing confidence in the repeatability of the radar measurements. To the west of Race Rocks, there is a strong cross-channel flow onto the Canadian shore; as the tide evolves, however, the cross-channel component weakens and flow becomes more aligned with the main axis of the strait. Northeast of Port Angeles, a distinct convergent front forms on each tide. In the last two maps (5b and 5c) a secondary front along a line due north of Ediz Hook is also apparent.

Finally, a map for the ebb phase of the tide is shown in Fig. 6. As the ebb sets in, a strong eddy forms east of Race Rocks, which persists for about 2-3 h, and a line of strong shear has developed tangentially to the northern side of the eddy. This shear line coincides approximately with a front frequently observed by boaters in this area. Moreover, offshore flows northeast of Ediz Hook form a convergent front in a similar position to that observed during floods, but with flows in the opposite direction.

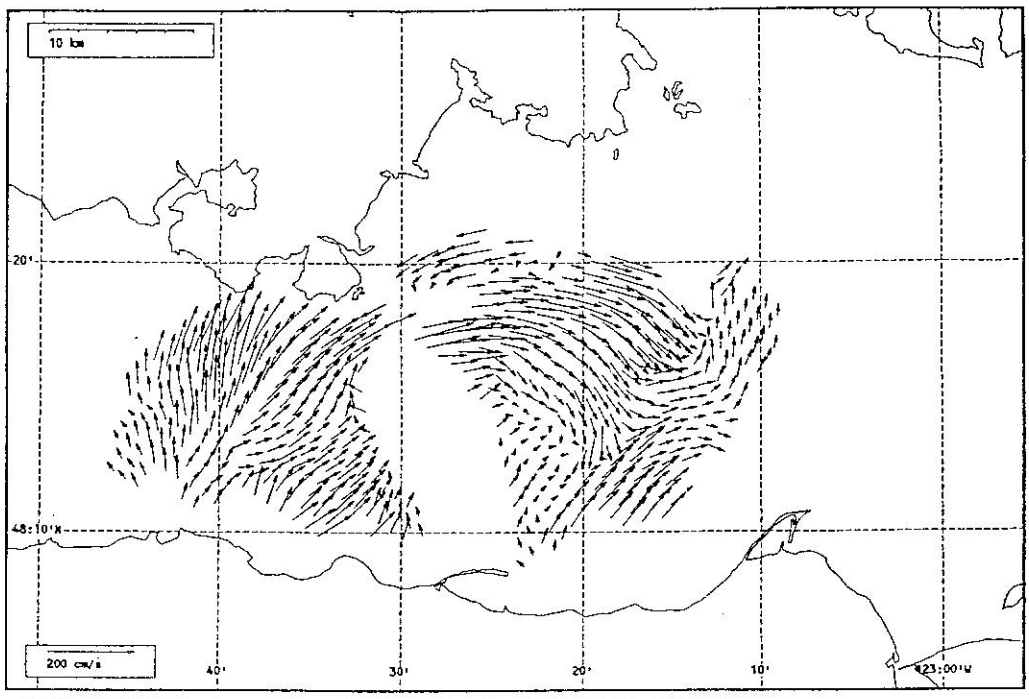

Total current vectors, Juan de Fuca Strait, 1992-07-11 22:00 Z.

Fig. 5a Flood tide current map, July 11, 1992 22:00 GMT.

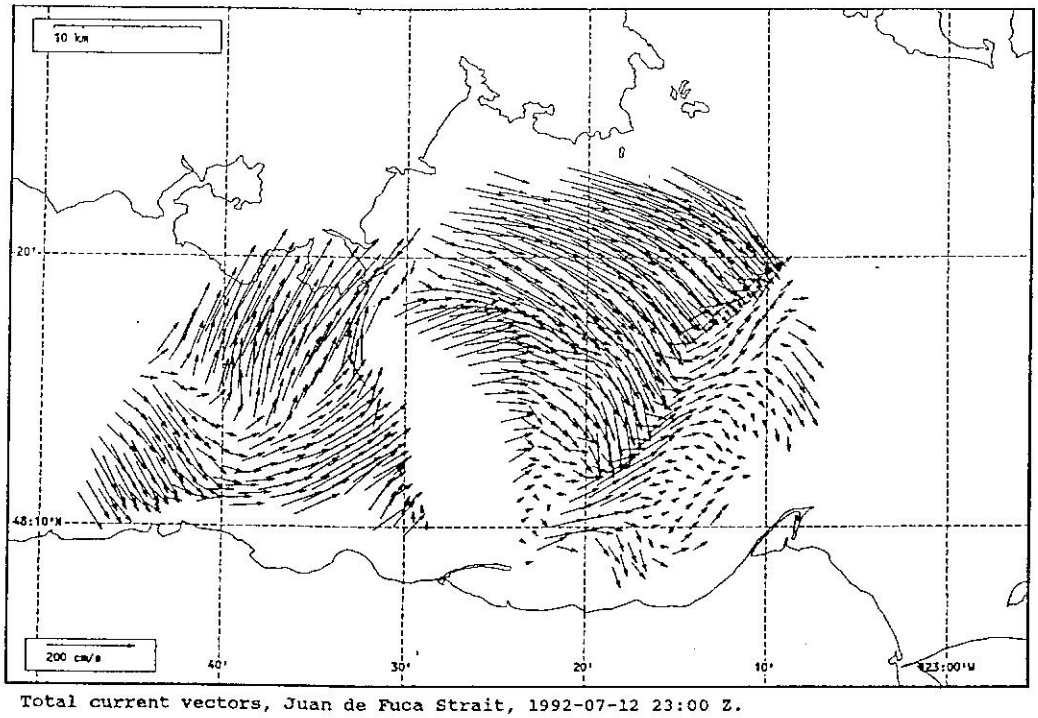

Total current vectors, Juan de Fuca Strait, 1992-07-12 23:00 Z.

Fig. 5b Flood tide current map, July 12, 1992 23:00 GMT.

These maps show the complex, small-scale yet spatially coherent patterns that develop, drawing their energy from non-linear interactions in the tidal flows. In waterways such as Juan de Fuca Strait, the energy associated with these sub-mesoscale features, such as meanders, fronts and eddies, is large.

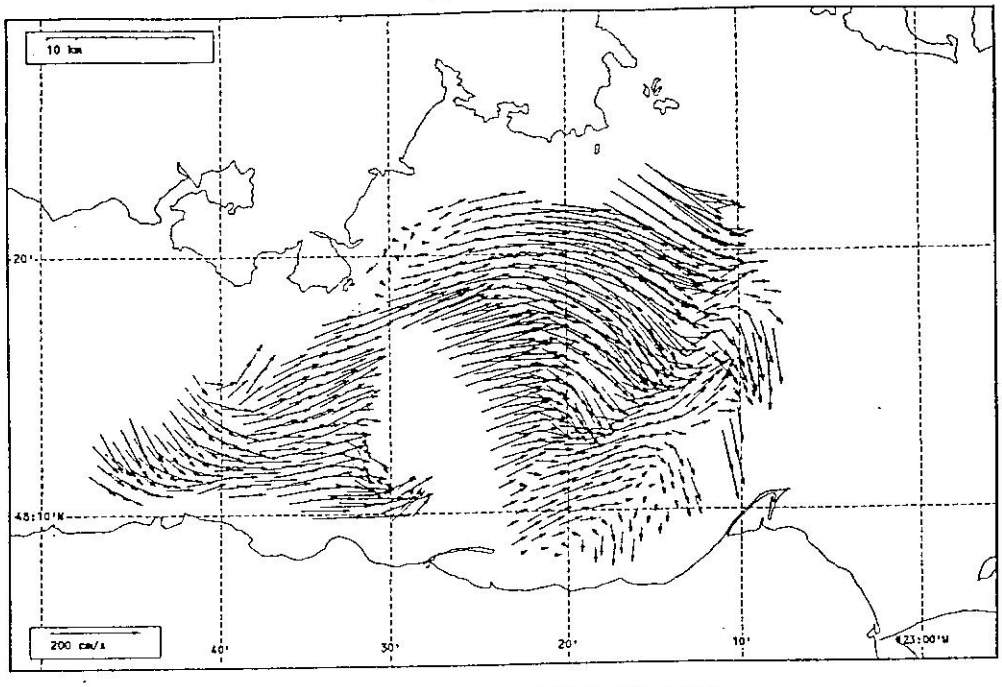

Fig. 5c. Flood tide current map, July 15, 1992 00:00 GMT.

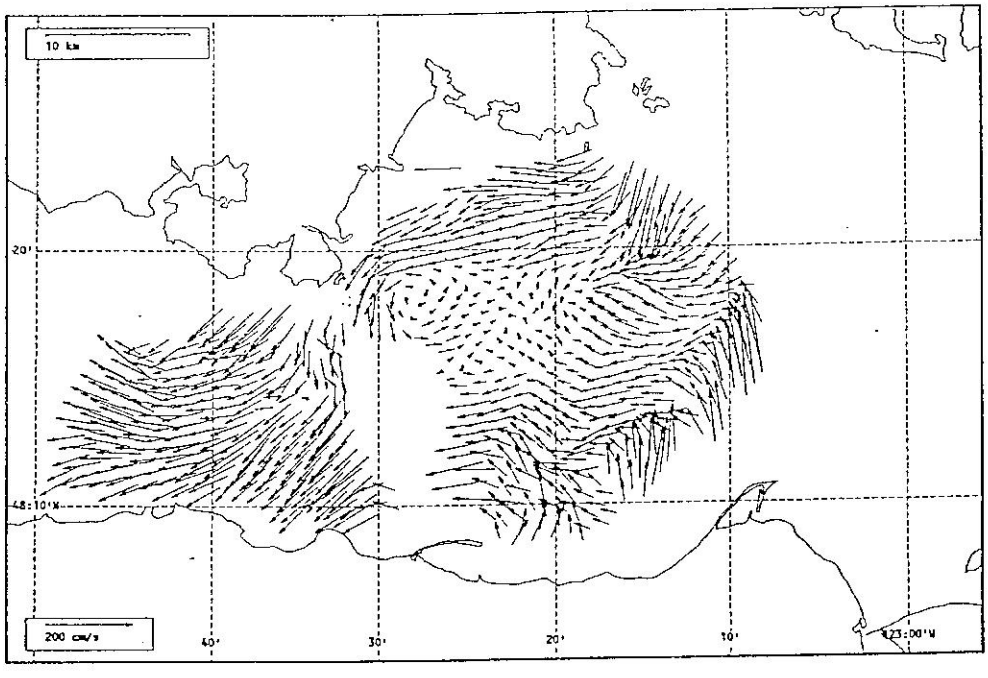

Fig. 6 Ebb tide current map, July 19, 1992 07:00 GMT.

Figure 7 illustrates one 9-day period of radar measurements in mid-channel, with the harmonic tidal signals superimposed. As can be seen here, the tide accounts for most of the energy in the signal. The difference between these two curves is the non-tidal residual, and much of the energy in this residual is present at high frequencies, arising from the short-lived, eddying and meandering motions. In this series, for example, the RMS velocity scales associated with the non-tidal residual are 35 cm/s and 18 cm/s for u and v respectively.

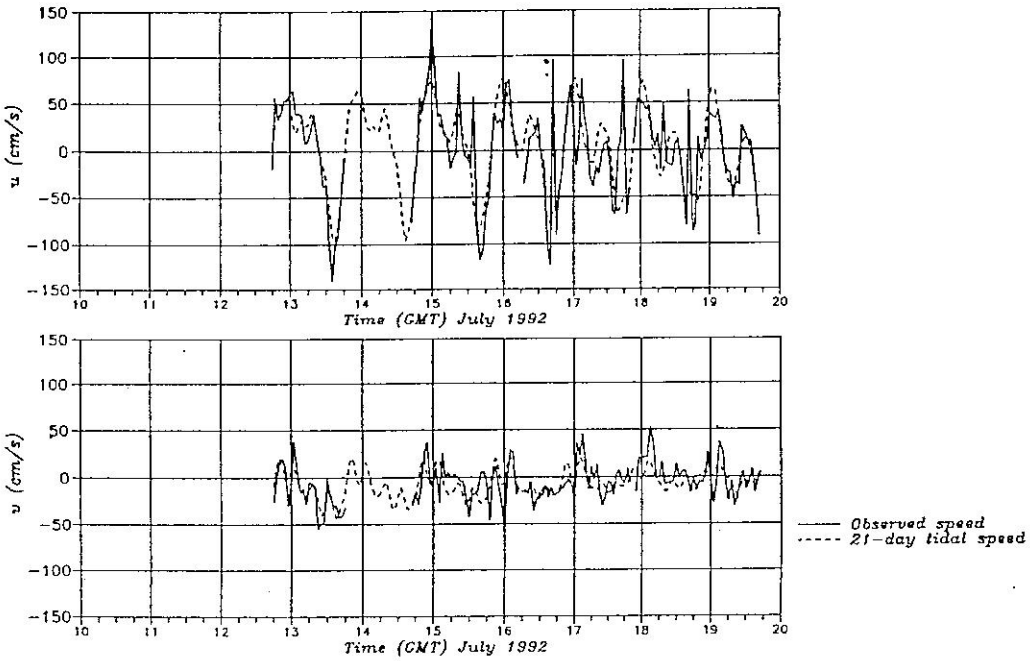

Fig. 7 Measured total and tidal (21-d analysis) current components.

5 CONCLUSIONS

The SeaSonde HF radar system successfully collected surface current data in Juan de Fuca Strait over a 21-day period once some of the early problems with power supply and antenna siting were solved. Despite heavy ship and boat traffic through the centre of the coverage area, including the regular ferry run from Port Angeles to Victoria, the ship removal algorithm worked well and there was no detectable data loss to ship spike interference. Similarly, little or no RF interference was noticed.

At 12.5 MHz maximum ranges varying from about 15 km to over 30 km. The sea echo returns at both radars were correlated with wind speed, which is consistent with better Bragg scattering wave heights at higher wind speeds. A higher transmit frequency, in the range of 20 to 30 MHz, is expected to achieve more consistent performance without a critical sacrifice in total range for the Straits of Juan de Fuca and Georgia. The higher frequency produces Bragg resonance from shorter waves that are likely to be more prevalent at lower winds in the inner waterway. The 12 to 13 MHz frequency range is expected to function well over more open-ocean conditions.

Analysis of the measured currents revealed a great deal of small-scale structure to the flows in this area, characterized by large shear in the current speeds. The SeaSonde parameters are not ideal for these conditions, and although hard to demonstrate, it is suspected that some features were under-resolved in more distant

range rings. An increase in HF radar resolution is thus warranted for this area, in terms of both range ring spacing and azimuth angle spacing.

A change in transmission frequency and range ring spacing can be accommodated with minor impact to the SeaSonde hardware design, and an improved method for radial current extraction at smaller angle increments can be made in software.

6 REFERENCES

Hardy, J.S., D.S. Dunbar and D.O. Hodgins, 1989. An Evaluation of Methods for Extracting Surface Currents from CODAR Data. Proc. IGARRS '89, 12th Canadian Symposium on Remote Sensing, Vancouver, Canada.

Hodgins, D.O., 1991. New Capabilities in Real-time Oil Spill and Fate Prediction Using HF Radar Remote Sensing. Proc. 14th AMOP Technical Seminar, June 12-14, 1991, Vancouver, Canada.

Hodgins, D.O., 1992. The SeaSonde High-frequency Radar System for Surface Current Measurements. Proc. 3rd ASEAN Science & Technology Week, Sept. 17-24, 1992, Singapore.

Hodgins, D.O. and J.S. Hardy, 1992a. Performance of the SeaSonde High-frequency Radar System for Surface Current Measurements. Proc. 15th AMOP Technical Seminar, June 10-12, 1992, Edmonton, Canada.

Hodgins, D.O. and J.S. Hardy, 1992b. Surface Current Data from Queen Charlotte Sound, B.C., Intercomparison of SeaSonde and Drifter Current Observations. Prepared for Fisheries & Oceans, Canada, Canadian Coast Guard, and Environment Canada by Seaconsult Marine Research Ltd.

Hodgins, D.O. J.H. Huang and M.F. Fingas, 1992. Oil Spill Modelling Using remote Sensed Surface Currents. Proc. Arctic and Marine Oilspill Program (AMOP) Technical Seminar, June 1992, Edmonton, 381-405.

Leise, J.A., 1984. The Analysis and Digital Signal Processing of NOAA's Surface Current Mapping System, *IEEE J. Ocean. Eng.*, **OE-9**(2), 106-113.

Lipa, B.J. and D.E. Barrick, 1983. Least-Squares Methods for the Extraction of Surface Currents From CODAR Crossed-Loop Data: Application at ARSLOE. IEEE *J. Oceanic Eng.*, OE-8(4), 226-253.